NASA Technical Memorandum 106355
ICOMP–93–33; CMOTT–93–12
AIAA–93–3051

Higher-Order Accurate Osher Schemes With Application to Compressible Boundary Layer Stability

J.J.W. Van Der Vegt
Institute for Computational Mechanics in Propulsion
and Center for Modeling of Turbulence and Transition
Lewis Research Center
Cleveland, Ohio

Prepared for the
AIAA 24th Fluid Dynamics Conference
sponsored by the American Institute of Aeronautics and Astronautics
Orlando, Florida, July 6–9, 1993

NASA

Higher-Order Accurate Osher Schemes with Application to Compressible Boundary Layer Stability

J. J. W. Van Der Vegt
Institute for Computational Mechanics in Propulsion
and Center for Modeling of Turbulence and Transition
Lewis Research Center, Cleveland, Ohio

Abstract

Two fourth order accurate Osher schemes are presented which maintain higher order accuracy on non-uniform grids. They use either a conservative finite difference or finite volume discretization. Both methods are successfully used for direct numerical simulations of flat plate boundary layer instability at different Mach numbers. Results of growth rates of Tollmien- Schlichting waves compare well with direct simulations of incompressible flow and for compressible flow with results obtained by solving the parabolic stability equations.

1. Introduction

The study of boundary layer stability and transition to turbulence is one of the classical topics in fluid mechanics. Linear and weakly non-linear theory, together with experiments, have been successful in describing several of the important instability mechanisms in compressible boundary layers, e.g. Tollmien-Schlichting (TS) waves, or first modes, and higher modes, which come into play at supersonic Mach numbers, Mack[15], and theory was also successful in describing secondary instability, Herbert[10].

The complicated phenomena in the non-linear stages, leading to transition and turbulence, however, require further understanding. Direct numerical simulations can provide some of this information, but their application to compressible boundary layers has been hindered by many obstacles. To mention just a few, high order accuracy is required on non-uniform grids and a severe time step limitation is encountered due to the small grid spacing in the boundary layer when using an explicit time integration method; whereas with implicit time integration methods it is difficult to maintain time accuracy.

Member AIAA

Spectral methods have been very successful in simulating incompressible flows in simple geometries, such as channel flow, e.g. Laurien and Kleiser[11], but are not easily extended to more complicated geometries. The recently popular compact finite difference schemes, Lele[13], do not have the geometric limitations of spectral methods and have been successfully applied to mixing layers and shock turbulence interaction, Lee et al[14]. Unfortunately, compact finite difference schemes and also spectral methods, cannot capture shocks and if they appear they have to be fully resolved, which can require prohibitively small grid spacings, Lee et al.[14].

There have been several attempts to use finite difference schemes for direct simulation of transition in compressible boundary layers. The most frequently used method is the fourth order accurate version of Mac Cormack's scheme, developed by Gottlieb and Turkel[7], e.g. Maestrello et al.[16] and Bestek et al.[3]. This method can only achieve higher order accuracy on grids generated as the product of two or more one-dimensional analytic transformations, limiting its applicability to relatively simple, smooth flows.

Most frequently explicit time integration methods have been used, but for many transitional flows the Courant-Friedrichs-Lewy (CFL) time step limitation is not necessary to maintain time accuracy. Recently Rai and Moin[21] developed a numerical scheme which solves the compressible Navier-Stokes equations using a time accurate upwind biased implicit method and were able to simulate bypass transition. This method alleviates the time step limitation of explicit methods, but has as main drawback that it uses the non-conservative form of the Navier-Stokes equations and only allows grid stretching in one direction. The grid stretching, however, does not have to be analytically defined because the higher order finite difference approximations are generated numerically in physical space.

In this paper two alternative methods will be discussed. The first method is a higher order accurate extension of the MUSCL scheme, originally developed by Van Leer[27] as a second order accurate extension of Godunov schemes. The scheme is related to the multi-dimensional essentially non-oscillatory (ENO) schemes

developed by Casper and Atkins[4] and Harten et al.[9]. The second method is a higher order accurate upwind biased version of the Osher scheme, which maintains its high order accuracy on non-uniform grids. Higher order accurate Osher schemes were also discussed by Rai[20], but his method is only higher order accurate on a uniform grid.

The discussion in this paper will be restricted to smooth flows, but both schemes have been extensively tested for flows with shocks and other discontinuities in one-dimensional flows. A detailed discussion of the benefits and application of these schemes to non-smooth flows can be found in Van Der Vegt[25]. The purpose of this paper is to investigate if these methods are accurate and efficient enough to be used as tools for direct simulation of boundary layer instability and transition to turbulence.

The finite volume scheme has as main benefits that it is a truly multi-dimensional scheme, whereas the finite difference scheme uses dimensional splitting. The finite volume scheme automatically satisfies conservation and is most closely related to the integral formulation of the compressible Euler and Navier-Stokes equations. It also maintains higher order accuracy at sonic points, which is not true for the finite difference formulation. The finite volume method, however, is slightly more costly than the finite difference scheme and requires significantly more effort to implement.

The use of an upwind scheme is beneficial for direct simulations of compressible flow, because it automatically controls aliasing errors. There are two types of upwind schemes, those based on flux vector splitting, e.g. Van Leer[28] and Steger-Warming[24], and those based on a Godunov approach which use the solution of a Riemann problem. Godunov schemes most closely mimic the physics of wave propagation in compressible flow and have excellent shock capturing properties. In this class of schemes the Roe and Osher approximate Riemann solvers are the most popular, see Roe[22] and Osher and Solomon[18]. The Osher scheme has been chosen because it has a very low numerical dissipation in boundary layers, which is crucial for direct simulations, and it has a continuously differentiable flux, which is important for implicit schemes. In addition it satisfies the entropy condition and has good shock capturing properties.

In the next two sections of this paper first the basic equations will be discussed and the higher order accurate numerical schemes will be presented. The paper will conclude with a discussion of the results of computations of boundary layer instability at various Mach numbers.

2. Navier-Stokes Equations

The Navier-Stokes equations can be considered either in integral formulation, leading to the finite volume discretization, or in differential form, which is the basis for the finite difference discretization. The finite volume method automatically satisfies the conservation properties of the equations but care has to be taken that the finite difference method is in the so-called conservation form. It is otherwise not possible to obtain a weak solution with the proper jump relations at discontinuities in the limiting case of vanishing viscosity, as demonstrated by Lax and Wendroff[12]. A detailed discussion of finite volume and finite difference methods and their differences can be found in Vinokur[29].

The integral formulation of the compressible Navier-Stokes equations is defined as:

$$\int_{\Omega(t_2)} \mathbf{U} dV - \int_{\Omega(t_1)} \mathbf{U} dV + \int_{t_1}^{t_2} \oint_{\partial\Omega(t)} \mathcal{F}(\mathbf{U}) \cdot \mathbf{n} dS dt = 0 \tag{2.1}$$

Here $\Omega(t)$ is the flow domain with boundary $\partial\Omega(t)$ at time t and $\mathbf{n}$ the unit outward normal vector at $\partial\Omega$. The vector $\mathbf{U}$ represents the conserved variables: $(\rho, \rho u, \rho v, \rho w, e)^T$, with ρ density, $\mathbf{u} = (u, v, w)^T$ the Cartesian velocity components, and e total energy. The matrix $\mathcal{F}$, which represents the fluxes through the surface $\partial\Omega(t)$, consists of two parts, F the inviscid flux, and V the viscous flux, with $\mathcal{F}$=F-V. The inviscid flux contribution F has as components:

$$\mathbf{F}_1 = \begin{pmatrix} \rho u \\ \rho u^2 + p \\ \rho uv \\ \rho uw \\ (e+p)u \end{pmatrix}; \quad \mathbf{F}_2 = \begin{pmatrix} \rho v \\ \rho uv \\ \rho v^2 + p \\ \rho vw \\ (e+p)v \end{pmatrix}$$

$$\mathbf{F}_3 = \begin{pmatrix} \rho w \\ \rho uw \\ \rho vw \\ \rho w^2 + p \\ (e+p)w \end{pmatrix} \tag{2.2}$$

where the dimensionless pressure p is determined from the equation of state: $p = \rho c_v T/(\gamma M^2)$, with c_v the specific heat at constant volume, γ the ratio of specific heat at constant pressure and constant volume, M the Mach number and T temperature. The temperature T is given by the relation: $T = \gamma(\gamma-1)M^2(e - \frac{1}{2}\rho \mathbf{u} \cdot \mathbf{u})/(\rho c_v)$.

The viscous contribution V has as components:

$$\mathbf{V}_1 = \begin{pmatrix} 0 \\ \tau_{xx} \\ \tau_{xy} \\ \tau_{xz} \\ \beta_x \end{pmatrix} \quad \mathbf{V}_2 = \begin{pmatrix} 0 \\ \tau_{xy} \\ \tau_{yy} \\ \tau_{yz} \\ \beta_y \end{pmatrix} \quad \mathbf{V}_3 = \begin{pmatrix} 0 \\ \tau_{xz} \\ \tau_{yz} \\ \tau_{zz} \\ \beta_z \end{pmatrix} \tag{2.3}$$

with the stress tensor τ and the variables β_x, β_y and β_z defined as:

$$\begin{aligned}
\tau_{xx} &= \left((2\mu + \lambda)\frac{\partial u}{\partial x} + \lambda(\frac{\partial v}{\partial y} + \frac{\partial w}{\partial z}) \right) / Re \\
\tau_{xy} &= \left(\mu(\frac{\partial u}{\partial y} + \frac{\partial v}{\partial x}) \right) / Re \\
\tau_{xz} &= \left(\mu(\frac{\partial u}{\partial z} + \frac{\partial w}{\partial x}) \right) / Re \\
\tau_{yy} &= \left((2\mu + \lambda)\frac{\partial v}{\partial y} + \lambda(\frac{\partial u}{\partial x} + \frac{\partial w}{\partial z}) \right) / Re \\
\tau_{yz} &= \left(\mu(\frac{\partial w}{\partial y} + \frac{\partial v}{\partial z}) \right) / Re \\
\tau_{zz} &= \left((2\mu + \lambda)\frac{\partial w}{\partial z} + \lambda(\frac{\partial u}{\partial x} + \frac{\partial v}{\partial y}) \right) / Re
\end{aligned} \tag{2.4}$$

$$\begin{aligned}
\beta_x &= u\tau_{xx} + v\tau_{xy} + w\tau_{xz} + \frac{\kappa}{(\gamma - 1)M^2 Pr}\frac{\partial T}{\partial x} \\
\beta_y &= u\tau_{xy} + v\tau_{yy} + w\tau_{yz} + \frac{\kappa}{(\gamma - 1)M^2 Pr}\frac{\partial T}{\partial y} \\
\beta_z &= u\tau_{xz} + v\tau_{yz} + w\tau_{zz} + \frac{\kappa}{(\gamma - 1)M^2 Pr}\frac{\partial T}{\partial z}
\end{aligned} \tag{2.5}$$

Here Re represents the Reynolds number, Pr Prandtl number, κ the coefficient of thermal conductivity and μ and λ the first and second viscosity coefficient. All computations were done using the relation $\lambda = -\frac{2}{3}\mu$, with μ given by Sutherland's law. The non-dimensional variables are defined with respect to the freestream velocity, density, temperature, viscosity, thermal conductivity and specific heat.

If we assume that all variables are continuously differentiable in time it is possible to rewrite equation (2.1) into:

$$\frac{\partial}{\partial t}\int_{\Omega(t)} \mathbf{U} dV + \oint_{\partial\Omega(t)} \mathcal{F}(\mathbf{U}) \cdot \mathbf{n} dS = 0 \tag{2.6}$$

A special constraint can be derived from this expression, namely the geometric conservation law. Inserting a uniform flow field in equation (2.6) we obtain:

$$\oint_{\partial\Omega(t)} \mathbf{n} dS = 0 \tag{2.7}$$

which states that the cell face $\partial\Omega(t)$ must be closed. When dividing the total flow field in a set of non-overlapping cells this constraint puts limitations on the way how to compute the cell faces and volumes. They all have to add up to the total volume and each cell will have to be closed otherwise a uniform flow field will be disturbed due to contributions from the metrics. This is a non-trivial problem when deriving higher order schemes and will be discussed in the next sections.

The differential form of the compressible Navier-Stokes equations is directly obtained from the integral formulation, equation (2.6), using Gauss' theorem and considering an arbitrary volume Ω:

$$\frac{\partial \mathbf{U}}{\partial t} + \nabla \cdot \mathcal{F}(\mathbf{U}) = 0 \tag{2.8}$$

This is the conservative formulation of the compressible Navier-Stokes equations and it is important that the discretization also can be written in conservation form. The geometric conservation law must be satisfied and this requires great care in dealing with the metrical coefficients in a finite difference discretization, especially in three dimensions.

3. Higher Order Accurate Finite Volume Scheme

Second order accurate finite volume schemes have been around for a long time. When extending the accuracy beyond second order several problems are encountered. It is no longer valid to equate cell averaged values with values at the cell center and a more elaborate algorithm to reconstruct point values from cell averaged values is required. In addition one has to compute the integrals of the fluxes over the cell surfaces more accurately. The standard procedure of multiplying the flux with the cell surface is only second order accurate. The geometry in a higher order accurate finite volume method also has to be represented more accurately, especially at the boundary. The relations for cell area and volume as given by Vinokur[29] are no longer sufficient. They are exact for hexahedrons with straight line edges, but not for cells with curved edges.

Until now very few attempts have been made to develop higher order accurate finite volume methods. For structured grids Harten et al.[9] and Casper and Atkins[4] developed the multi-dimensional ENO schemes and Abgrall[1] and Harten and Chakravarthy[8] studied these schemes for unstructered grids. Despite the fact that the unstructured approach has more flexibility in treating complicated geometries and allows local grid refinement it was decided to use the structured grid approach developed by Casper and Atkins[4]. Both CPU

time and memory usage in the unstructered schemes, is so large that it is not feasible to use these methods for direct or large eddy simulations of compressible flow. The structured grid approach, however, requires a smooth C^3 grid. It is possible to deal with locally non-smooth boundaries and intersections in the finite volume approach by subdividing the grid into smooth subsections using a multi-block approach. The smoothness requirements of the grid will limit the application of this method to fairly simple geometries, but due to their high cost large eddy and direct simulations will be limited to simple flows for quite a while. The finite volume method is, however, considerably more flexible than spectral methods which require a C^∞ grid.

The use of a structured grid makes it possible to transform the physical domain to a simpler computational domain. Let ξ, η, and ζ be the coordinates in the computational domain then they are related to the physical coordinates x, y, z by the relations:

$$\begin{aligned} \xi &= \xi(x,y,z) \\ \eta &= \eta(x,y,z) \\ \zeta &= \zeta(x,y,z) \end{aligned} \tag{3.1}$$

The finite volume discretization on a structured grid is obtained by dividing the domain Ω into a regular partition $\Omega_{i,j,k}$. Each element $\Omega_{i,j,k}$ is a hexahedron with coordinates x_i, y_j and z_k for the top right corner. The subdomains $\Omega_{i,j,k}$ are non-overlapping and their sum is equal to the domain Ω.

The cell average $\overline{\mathbf{U}}_{i,j,k}$ in a cell with index (i,j,k) is defined as:

$$\overline{\mathbf{U}}_{i,j,k} = \frac{1}{Vol(\Omega_{i,j,k})} \int_{\Omega_{i,j,k}} \mathbf{U} dV \tag{3.2}$$

with $Vol(\Omega_{i,j,k})$ the volume of cell $\Omega_{i,j,k}$. The equation for the cell average is obtained by limiting the integration domain Ω to $\Omega_{i,j,k}$ in equation (2.6), and is equal to:

$$\frac{\partial}{\partial t}\overline{\mathbf{U}}_{i,j,k}(t) + \mathbf{h}_{i,j,k}(\mathbf{U}) = 0 \tag{3.3}$$

with the flux integral $\mathbf{h}_{i,j,k}$ at the surface $\partial\Omega_{i,j,k}$ of the cell $\Omega_{i,j,k}$ defined as:

$$\begin{aligned} \mathbf{h}_{i,j,k}(\mathbf{U}) &= \frac{1}{Vol(\Omega_{i,j,k})} \int_{\partial\Omega_{i,j,k}} \mathcal{F}(\mathbf{U}) \cdot \mathbf{n} dS \\ &\equiv \frac{1}{Vol(\Omega_{i,j,k})} \int_{\partial\Omega_{i,j,k}} \hat{\mathbf{F}}(\mathbf{U}) dS \end{aligned} \tag{3.4}$$

with $\hat{\mathbf{F}}$ the flux normal to the cell surface:

$$\hat{\mathbf{F}} = k_1\mathbf{F}_1 + k_2\mathbf{F}_2 + k_3\mathbf{F}_3 \tag{3.5}$$

and $\mathbf{n} = (k_1, k_2, k_3)^T$. This relation gives the method of lines formulation for the cell averaged equation $\overline{\mathbf{U}}_{i,j,k}(t)$. The numerical flux in a higher order finite volume scheme now is constructed such that it approximates the exact flux at time $t = (n+1)\Delta t$ up to $O(h^r)$:

$$\overline{\mathbf{U}}^{n+1}_{i,j,k} - \left[\overline{E}_h(\Delta t) \cdot \overline{\mathbf{U}}^n\right]_{i,j,k} = O(h^r) \tag{3.6}$$

with $\overline{E}_h(\Delta t)$ the numerical solution operator. The higher order accurate finite volume scheme therefore gives an r-th order accurate approximation to the cell averages, not the point values as in a finite difference scheme.

The two important ingredients of a higher order accurate finite volume method are the reconstruction of the point values $\mathbf{U}(\mathbf{x})$ from the cell averaged values $\overline{\mathbf{U}}_{i,j,k}$ and the computation of the flux $\hat{\mathbf{F}}$ at the cell face. The point values are necessary to compute the fluxes $\mathbf{h}_{i,j,k}$ at the cell faces which depend on $\mathbf{U}(\mathbf{x})$ and not on $\overline{\mathbf{U}}$. This is done with the reconstruction method discussed in section 3.1. The fluxes at the cell faces are computed by considering a Riemann problem at each cell face. This method was introduced by Godunov[6] for first order accurate schemes and extended by Van Leer[27] to second order accuracy. Instead of using the exact solution of the Riemann problem the approximate Riemann solver developed by Osher and Solomon[18] is used, because it is less expensive than the exact solution, but has excellent shock capturing properties and minimal dissipation in boundary layers.

3.1 Reconstruction of Point Values from Cell Averages

In one dimension the most successful reconstruction technique is based on the primitive function method, see e.g. Harten et al.[9]. This method was extended by Harten et al.[9] and Casper and Atkins[4] to multiple dimensions using the one-dimensional primitive function reconstruction technique first to compute line averages from cell averages, after which point values are computed with a second one-dimensional reconstruction. It is, however, possible to define a primitive function directly for the multi-dimensional problem without having to use one-dimensional primitive functions.

Define the primitive function $\mathcal{U}$ as:

$$\mathcal{U}(\xi,\eta,\zeta) = \int_{\zeta_0}^{\zeta}\int_{\eta_0}^{\eta}\int_{\xi_0}^{\xi} \mathbf{U}(\xi',\eta',\zeta')|J(\xi',\eta',\zeta')| d\xi' d\eta' d\zeta' \tag{3.7}$$

then the flow field $\mathbf{U}$ satisfies the relation

$$\mathbf{U}(\xi,\eta,\zeta) = \frac{1}{|J(\xi,\eta,\zeta)|} \frac{\partial^3}{\partial\zeta\partial\eta\partial\xi}\mathcal{U}(\xi,\eta,\zeta) \tag{3.8}$$

with ξ, η and ζ the coordinates in computational space and J the Jacobian of the coordinate transformation. The primitive function $\mathcal{U}$ can be related to the cell average $\overline{\mathbf{U}}$ in physical space using the following relation:

$$\begin{aligned}\mathcal{U}(\xi_i,\eta_j,\zeta_k) &= \int_{\zeta_0}^{\zeta_k}\int_{\eta_0}^{\eta_j}\int_{\xi_0}^{\xi_i}\mathbf{U}|J|d\xi' d\eta' d\zeta' \\ &= \sum_{k'=k_0}^{k}\sum_{j'=j_0}^{j}\sum_{i'=i_0}^{i}\int_{k'-1}^{k'}\int_{j'-1}^{j'}\int_{i'-1}^{i'}\mathbf{U}|J|d\xi' d\eta' d\zeta' \\ &= \sum_{k'=k_0}^{k}\sum_{j'=j_0}^{j}\sum_{i'=i_0}^{i}\int_{\Omega_{i',j',k'}}\mathbf{U}(\mathbf{x},t)dV \\ &= \sum_{k'=k_0}^{k}\sum_{j'=j_0}^{j}\sum_{i'=i_0}^{i} Vol(\Omega_{i',j',k'})\overline{\mathbf{U}}_{i',j',k'}\end{aligned} \tag{3.9}$$

This relation is the basis for the higher order finite volume scheme. It defines the primitive function $\mathcal{U}$ directly at the corners of each hexahedron in computational space (ξ_i,η_j,ζ_k) and is conservative. The point values $\mathbf{U}(\mathbf{x})$ are then obtained using equation (3.8).

When the flow field is smooth the following procedure can be used to compute the pointwise data: For a surface in the plane $\xi=\xi^*$, first approximate the left and right states by differentiating the primitive function $\mathcal{U}$ with upwind biased differences in both ξ-directions with fourth order accuracy for all indices j and k. Then the η and ζ-derivates are computed at the Gauss quadrature points and divided by the local Jacobian to obtain the point values. This process is repeated for the planes with $\eta=\eta^*$ and $\zeta=\zeta^*$ and works well for smooth flows. For flows with discontinuities the ENO reconstruction, which tries to use only data from the smooth part of the flow field has to be used. This will be discussed in a future paper.

Although this process is rather simple care has to be taken to prevent loss of accuracy due to truncation errors, because the primitive function $\mathcal{U}$ frequently becomes very large or small. The way to prevent this is to construct the primitive function using only those cells around the cell with index (i,j,k) which are needed to compute the derivatives in equation (3.8) and dynamically adapt the indices i_0, j_0 and k_0. Accuracy is further improved by combining the process of summation and differentiation, e.g. first compute the sum with i-index, then differentiate this result and compute the summation with j-index, and so on.

In order to preserve uniform flow it is necessary to compute the Jacobian of the coordinate transformation at the Gauss quadrature points the same way as done for the flow field U. This can be accomplished most easily by multiplying equation (3.8) with the Jacobian and inserting a uniform flow field in equations (3.8-9) will give the Jacobian at the Gauss quadrature points with the same reconstruction process as for $\mathbf{U}$. This procedure is important because otherwise the reconstruction process will generate small errors which can be very annoying on stretched grids.

3.2 Higher Order Accurate Flux Integrals

The discretization of the integral formulation of the compressible Navier-Stokes equations (3.3) is completed with the approximation of the flux integrals given by equation (3.4). Casper and Atkins[4] gave a detailed analysis of the accuracy required in the reconstruction problem and the computation of the flux integrals to obtain an accurate solution with an error of order h^r. In this paper we limit the discussion to fourth order accuracy. The use of a Gauss quadrature method is the most efficient way to compute the flux integrals with fourth order accuracy. First the integral over the cell boundary is split into the sum of integrals over the six cell faces:

$$\mathbf{h}_{i,j,k}(\mathbf{U}) = \frac{1}{Vol(\Omega_{i,j,k})}\sum_{l=1}^{6}\int_{\partial\Omega^l_{i,j,k}}\hat{\mathbf{F}}(\mathbf{U})dS \tag{3.10}$$

here the index l refers to one of the six faces of the hexahedron. Then the flux integrals at each cell face can be further evaluated using the Gauss quadrature rule at each cell face and the Osher approximate Riemann solver[17,18] is used to compute the flux at each quadrature point:

$$\begin{aligned}&\int_{\partial\hat{\Omega}^l_{i,j,k}}\hat{\mathbf{F}}(\mathbf{U})dS = \\ &=\frac{1}{2}\int_{\partial\hat{\Omega}^l_{i,j,k}}\left(\hat{\mathbf{F}}_L+\hat{\mathbf{F}}_R-\int_{\Gamma}|\partial\hat{\mathbf{F}}|dU\right)|J|d\hat{S} \\ &\cong\frac{1}{8}\sum_{m=1}^{4}\left(\hat{\mathbf{F}}_L+\hat{\mathbf{F}}_R-\int_{\Gamma}|\partial\hat{\mathbf{F}}|dU\right)_{g_{m,l}}|J_{g_{m,l}}|d\hat{S}\end{aligned} \tag{3.11}$$

with $\partial\hat{\Omega}^l_{i,j,k}$ the cell face with index l in computational space. The indices $g_{m,l}$ refer to the quadrature points with index m in the cell face where the fluxes of the left and right states $\mathbf{F}_{L,R}$ and the Osher path integral are computed. The quadrature points have coordinates $(\frac{1}{2}\pm\frac{1}{2}\sqrt{\frac{1}{3}},\frac{1}{2}\pm\frac{1}{2}\sqrt{\frac{1}{3}})$, assuming that the hexahedrons sides have unit length. This relation is used by Casper

and Atkins[4] and requires four calculations of the approximate Riemann flux for each cell face which significantly increases the computing time. Harten and Chakravarthy[8] suggested that only one computation of the (approximate) Riemann flux is required to maintain accuracy in smooth flows. Due to the fact that the Riemann flux, and also the approximate Riemann flux according to Osher, is Lipschitz continuous and $|\mathbf{U}_L - \mathbf{U}_R| = O(h^r)$ in smooth flows it is easy to show that the third component in the integral, equation(3.11), can be approximated as:

$$\int_{\partial\hat{\Omega}^1_{i,j,k}} \int_{\Gamma} |\partial\hat{\mathbf{F}}| dU |J| d\hat{S} = \int_{\Gamma} |\partial\hat{\mathbf{F}}_{c_l}| dU |J_{c_l}| + O(h^r) \tag{3.12}$$

Here the index c_l refers to center of the cell face with index l. This relation significantly reduces the computing time, while maintaining the total accuracy at the slight expense of computing $\mathbf{U}_{L,R}$ at the cell face center. In regions with discontinuities it is, however, advisable to use the (approximate) Riemann solution at all the Gauss quadrature points.

4. Higher Order Accurate Finite Difference Scheme

The most difficult problem in deriving a higher order accurate finite difference scheme is to find a way to maintain that accuracy on a non-uniform grid. In upwind finite difference schemes, either based on flux vector splitting or using approximate Riemann solvers, the flux is a function of more than one grid point. When deriving the expression for the higher order differences care has to be taken to account for the changing metrics, but this is frequently neglected. For instance the higher order Osher scheme derived by Rai[20] is only higher order accurate on a uniform grid. In addition to the accuracy requirement care has to be taken that the scheme is in conservation form and maintains uniform flow, which is a non-trivial requirement for a finite difference scheme. The conservation property is important on physical grounds, the equations express conservation of mass, momentum and energy, but is also important when dealing with discontinuities. In this paper, however, only smooth flow fields will be considered.

Before deriving the higher order Osher scheme it is necessary to study the first order Osher scheme in more detail . The conservative approximation to $\partial_\xi \hat{\mathbf{E}}$ using Osher's scheme is defined as:

$$\partial_\xi \hat{\mathbf{E}}_i = \frac{1}{\Delta\xi}(\hat{\mathbf{E}}_{i+\frac{1}{2}} - \hat{\mathbf{E}}_{i-\frac{1}{2}}) \tag{4.1}$$

where the conservative flux is defined as:

$$\hat{\mathbf{E}}_{i+\frac{1}{2}} = \frac{1}{2}(\hat{\mathbf{E}}_{i+1}(\xi_{i+\frac{1}{2}}) + \hat{\mathbf{E}}_i(\xi_{i+\frac{1}{2}}) - \int_{\Gamma_i} \partial_{\mathbf{U}}\hat{\mathbf{E}}^+(\xi_{i+\frac{1}{2}})d\mathbf{U} + \int_{\Gamma_i} \partial_{\mathbf{U}}\hat{\mathbf{E}}^-(\xi_{i+\frac{1}{2}})d\mathbf{U}) \tag{4.2}$$

with equivalent relations for $\partial_\eta \hat{\mathbf{F}}$ and $\partial_\zeta \hat{\mathbf{G}}$. The symbol $\partial_{\mathbf{U}}$ represents partial differentiation with respect to $\mathbf{U}$ and for ease of notation the j and k indices are omitted. In this relation $\xi_{i+\frac{1}{2}}$ refers to the metrical coefficients which are computed at the point with index $i+\frac{1}{2}$. The integrals in equation (4.2) are computed along a path in phase space, Γ_i, and using the fact that the Riemann invariants are constant along this path Osher was able to derive exact analytic expressions for these integrals, see[20,22]. It is important to note that although the path integral Γ_i is from i to $i+1$ only metrical coefficients at one point must be used for consistency. As can be seen directly from equation (4.2), the flux $\hat{\mathbf{E}}_{i+\frac{1}{2}}$ depends on the positions with indices i, $i+\frac{1}{2}$ and $i+1$. Using a Taylor series expansion with respect to both i and $i+1$ Rai[20] was able to derive higher order conservative expressions for $\partial_\xi \hat{\mathbf{E}}_i$. The dependency on $i+\frac{1}{2}$, however, was neglected, which reduces the order of accuracy of the scheme on a non-uniform grid, even on mildly stretched grids The analytical derivations necessary to obtain Rai's higher order Osher scheme are already tedious and taking care of the changing metrical coefficients, which would require Taylor series expansions up to at least fourth order in three independent variables, becomes unwieldy.

An alternative is to compute the higher order accurate flux approximations numerically. This is done using the flux-ENO scheme discussed in Van Der Vegt[25], but the stencil switching, which is part of ENO schemes, is eliminated in this paper. As starting point a different formulation of the first order Osher scheme is used:

$$\partial_\xi \hat{\mathbf{E}}_i = \int_{\Gamma_{i-1}} \partial_{\mathbf{U}}\hat{\mathbf{E}}^+(\xi_{i-\frac{1}{2}})d\mathbf{U} + \int_{\Gamma_i} \partial_{\mathbf{U}}\hat{\mathbf{E}}^-(\xi_{i+\frac{1}{2}})d\mathbf{U} \tag{4.3}$$

It is easy to show that both formulations are equivalent, see Osher and Solomon[18]. The higher order scheme is derived using a Newton interpolation to the fluxes. The Newton interpolation, however, cannot be directly applied to the integrals in equation (4.3) because of the path integrals. In order to use the Newton interpolation we use some simple relations, which were derived by Shu and Osher[23]: The function $\mathbf{f}(x)$ can always expressed as:

$$\mathbf{f}(x) = \frac{1}{\Delta x}\int_{x-\frac{\Delta x}{2}}^{x+\frac{\Delta x}{2}} \mathbf{h}(x')dx'$$

and using its primitive function: $\mathbf{F}(x) = \frac{1}{\Delta x}\int_{\infty}^{x} \mathrm{h}(x')dx'$ the following relation is obtained:

$$\mathbf{f}(x_i) = \mathbf{F}(x_i + \frac{\Delta x}{2}) - \mathbf{F}(x_i - \frac{\Delta x}{2}) \qquad (4.4)$$

These relations can be used to link the primitive function $\mathbf{F}$ to the flux integrals $\mathrm{df}_i^{\pm}$:

$$\begin{aligned}\mathrm{df}_i^{+} =& \mathbf{f}_i^{+} - \mathbf{f}_{i-1}^{+} \\ =& \mathbf{F}^{+}[x_{i+\frac{1}{2}}, x_{i-\frac{1}{2}}] - \mathbf{F}^{+}[x_{i-\frac{1}{2}}, x_{i-\frac{3}{2}}] \\ =& 2\mathbf{F}^{+}[x_{i+\frac{1}{2}}, x_{i-\frac{1}{2}}, x_{i-\frac{3}{2}}]\end{aligned} \qquad (4.5)$$

$$\begin{aligned}\mathrm{df}_i^{-} =& \mathbf{f}_{i+1}^{-} - \mathbf{f}_i^{-} \\ =& \mathbf{F}^{-}[x_{i+\frac{3}{2}}, x_{i+\frac{1}{2}}] - \mathbf{F}^{-}[x_{i+\frac{1}{2}}, x_{i-\frac{1}{2}}] \\ =& 2\mathbf{F}^{-}[x_{i+\frac{3}{2}}, x_{i+\frac{1}{2}}, x_{i-\frac{1}{2}}]\end{aligned} \qquad (4.6)$$

with:

$$\begin{aligned}\mathrm{df}_i^{-} &= \int_{\Gamma_i} \partial_{\mathbf{U}}\hat{\mathbf{E}}^{-}(\xi_{i+\frac{1}{2}})d\mathbf{U} \\ \mathrm{df}_i^{+} &= \int_{\Gamma_{i-1}} \partial_{\mathbf{U}}\hat{\mathbf{E}}^{+}(\xi_{i-\frac{1}{2}})d\mathbf{U}\end{aligned}$$

and $\mathbf{F}[x_{i+k}, \ldots, x_i]$ the k-th divided difference defined as:

$$\mathbf{F}[x_{i+k}, \cdots, x_i] = \frac{1}{k}(\mathbf{F}[x_{i+k}, \ldots, x_{i+1}] - \mathbf{F}[x_{i+k-1}, \ldots, x_i])$$

In the derivation of the higher order accurate scheme the specific functional form of the functions $\mathbf{f}^{\pm}$ and $\mathbf{F}^{\pm}$ is not needed, only their divided differences.

The primitive function $\mathbf{F}$ is now approximated with a fifth order Newton polynomial using the divided differences defined in eq. (4.5-6). The higher order divided differences can be easily obtained by further extending the divided difference tables given by equations (4.5-6). The nodes in the Newton interpolation are chosen such that an upwind biased scheme is obtained. This relation is then differentiated at: $x_{i+\frac{1}{2}}$:

$$\begin{aligned}\partial_\xi \mathbf{F}^{+}(x_{i+\frac{1}{2}}) =& \mathbf{F}^{+}[x_{i+\frac{1}{2}}, x_{i-\frac{1}{2}}] + \mathbf{F}^{+}[x_{i+\frac{1}{2}}, \cdots, x_{i-\frac{3}{2}}] \\ &+ 2\mathbf{F}^{+}[x_{i+\frac{3}{2}}, \cdots, x_{i-\frac{3}{2}}] \\ &- 2\mathbf{F}^{+}[x_{i+\frac{3}{2}}, \cdots, x_{i-\frac{5}{2}}]\end{aligned} \qquad (4.7)$$

$$\begin{aligned}\partial_\xi \mathbf{F}^{-}(x_{i+\frac{1}{2}}) =& \mathbf{F}^{-}[x_{i+\frac{3}{2}}, x_{i+\frac{1}{2}}] - \mathbf{F}^{-}[x_{i+\frac{5}{2}}, \cdots, x_{i+\frac{1}{2}}] \\ &+ 2\mathbf{F}^{-}[x_{i+\frac{5}{2}}, \cdots, x_{i-\frac{1}{2}}] \\ &+ 2\mathbf{F}^{-}[x_{i+\frac{7}{2}}, \cdots, x_{i-\frac{1}{2}}]\end{aligned} \qquad (4.8)$$

The higher order approximation to $\partial_\xi \hat{\mathbf{E}}_i$ is obtained using equation (4.4) and adding the positive and negative contributions in equations (4.7-8):

$$\partial_\xi \hat{\mathbf{E}}_i = \partial_\xi \mathbf{F}(x_{i+\frac{1}{2}}) - \partial_\xi \mathbf{F}(x_{i-\frac{1}{2}}) \qquad (4.9)$$

This relation is conservative, fourth order accurate, and maintains its higher order accuracy on a non-uniform grid because the change in metrical coefficients is properly taken care off by means of the Newton interpolation. It satisfies the geometrical conservation law because for each of the integrals $\mathrm{df}_i^{\pm}$, $i \in \{i-2, i+2\}$, appearing in the divided differences, the metrics are chosen at indices $i+\frac{1}{2}$, $i \in \{i-2, i+2\}$. The geometric conservation law then is automatically satisfied because for uniform flow each of the integrals gives a zero contribution independent of the metrical coefficients. The additional cost of computing the divided differences is negligible compared to the computation of the integrals $\mathrm{df}^{\pm}$ and the scheme is as efficient as a scheme with analytically derived coefficients. One additional remark must be made about the first divided difference in equations (4.7-8). Their value is unknown, but not needed, because in equation (4.9) only their difference is used, which is exactly the first order contribution and given by equations (4.5-6).

5. Implementation of Higher Order Schemes

In order to obtain the high accuracy necessary for direct simulations a large number of grid points is required. In order to efficiently run the program with such large grids a general three-dimensional multi-block code has been written. This gives more flexibility in managing the large memory requirements and it is easier to generate grids for more complicated geometries. The inviscid contribution in the compressible Navier-Stokes equations is discretized using the procedure described in the previous sections. The viscous terms are implemented using a fourth order accurate, conservative central differences for the finite difference scheme, but the viscous contribution is only second order accurate for the finite volume scheme. The development of a fourth order accurate viscous discretization for the finite volume scheme is currently in progress. Second order accurate implicit time integration is used and in order to maintain time accuracy a Newton procedure is chosen, equivalent to the one used by Rai and Moin[21] and Rai[20]. In this method the equations are discretized with all the fluxes computed at the new time level $n+1$. The resulting non-linear equations are linearized using a Newton procedure and the large system of linear equations is solved iteratively. In [20,21] the diagonal

form of approximate factorization according to Pulliam and Chaussee[19] was chosen, which only gives a crude approximation to the solution of the linear system. In this paper a more accurate iterative scheme based on the zebra line Gauss-Seidel method is used and for each step in the Newton procedure the system is solved up to machine accuracy. This method is used plane by plane and fits well into the Newton procedure.

The Newton procedure makes it possible to have an implicit spatial discretization which is of lower accuracy than the explicit part, but because each time step the Newton procedure is iterated time accuracy is maintained and the higher order spatial accuracy is preserved. Usually four Newton iterations are sufficient, but for convergence of the Newton scheme it is necessary to solve the linear system of the implicit time integration with high accuracy.

The Newton procedure requires the computation of the Jacobian of the flux vector, which is quite cumbersome to derive, especially for the viscous terms. Currently, both the exact Jacobian of the Osher fluxes and the approximation using the Jacobian of the Steger-Warming[24] flux vector splitting are used in the implicit time integration. The exact Jacobian of the Osher fluxes improves the convergence rate compared with the approximate Jacobian. It is, however, approximately three times more expensive to compute the exact Jacobian and for most cases the computing time for both schemes is about equal. For steady flows, where the Jacobian has to be updated only after a certain number of time steps the exact Jacobian is more efficient.

The boundary conditions for the Osher scheme are implemented using the procedure proposed by Osher and Chakravarty[17]. In this method a Riemann initial-boundary value problem is solved instead of an initial value problem, which is used in the interior of the domain. This method is very robust and elegant, but a significant effort is required to derive all relations to compute the boundary fluxes and Jacobians.

6. Results and Discussion

In this section results will be presented of two simulations of ribbon induced boundary layer instability to demonstrate the ability of the two numerical schemes discussed in this paper to accurately predict boundary layer instability and their possible use for simulations of turbulent and transitional boundary layers. Although the results in this section are all two dimensional the full three-dimensional discretization was used.

As a first step it is crucial to have extremely accurate solutions of the mean flow. In many previous studies an analytically defined mean flow was used, but this becomes difficult for flows in more general geometries. The use of an analytically defined mean flow also has as disadvantage that it does not exactly satisfy the discretized equations and will generate numerical transients.

In Figures 1 and 2 the mean flow profiles obtained with the finite difference scheme discussed in section 4 are plotted at 10 equally spaced stations with Re_x, the Reynolds number based on the distance from the nose of the plate, ranging from 50.000 to 320.000 versus the similarity parameter $\eta = \frac{y}{x}\sqrt{Re}$, with Re the Reynolds number based on plate length, x the streamwise distance from the nose of the plate and y the normal distance. The freestream Mach number is .08. The dimensionless normal velocity in Figure 2 is defined as: $\hat{v} = v\sqrt{Re_x}$. At the inlet a boundary layer solution was specified and the grid was chosen to approximately follow the streamlines and generated with the GridGen2d package. The grid is non-orthogonal in the interior and the normal grid spacing increases downstream. In the same plot also the compressible Blasius solution is plotted and it is clear that all lines completely collapse for the mean flow streamwise component, Figure 1. The same is true for the normal velocity, Figure 2, except for the asymptotic value outside the boundary layer, which is slightly higher than the Blasius solution. This slight difference is correct because in the boundary layer solution the small displacement of the boundary layer is not accounted for. The comparison between the theoretical and numerical solutions is remarkable considering the high Reynolds number of the base flow. Especially the accurate solution of normal velocity component is noteworthy, because its value is much smaller than the streamwise component and more difficult to compute. Most tests of numerical schemes on a flat plate boundary layer use a Reynolds number which is considerably lower and only show the streamwise velocity component. Accurate boundary layer profiles were already obtained with 35 points in the normal direction, but the total grid consisted of 336 $\times$ 80 points to provide sufficient accuracy for the direct simulations, discussed in the next part. This demonstrates that the Osher scheme is considerably more accurate in boundary layers than schemes based on flux vector splitting, Van Der Vegt[26].

The mean flow profiles obtained with the finite volume scheme discussed in section 3 are similar, but the finite volume scheme turns out to be more sensitive to the smoothness of the grid on highly stretched meshes. Care has to be taken that the grid for the finite volume scheme is at least three times differentiable. The sensitivity to the grid smoothness of the finite volume

scheme is caused by the fact that in the reconstruction process the cell averaged flow field $\overline{U}_{i,j,k}$ in equation (3.9) is multiplied with the cell volume. The cell volume changes much more rapidly than the grid spacing. The finite difference scheme is less sensitive to the grid, because it uses dimensional splitting and depends therefore only on the smoothness of the grid in each coordinate direction. The sensitivity to the grid smoothness of the finite volume scheme certainly needs further attention before this scheme can be used for more general applications.

Another problem when using a high order accurate scheme to obtain steady solutions for high Reynolds number flows is the slow convergence to steady state. Due to the minimal amount of numerical dissipation it takes a significant amount of computing time to eliminate all transients. Convergence to steady state was improved using an implicit scheme and CFL numbers between 1000 and 5000 were used to obtain steady results with the fourth order accurate schemes. In order to further speed up convergence the computations were started with a first order accurate scheme till the residue was significantly reduced, followed by the fourth order scheme till machine accuracy was obtained.

The first simulation of boundary layer instability is a comparison with the direct simulations of incompressible flow about a flat plate done by Fasel et al.[5]. All parameters were chosen as close as possible to the one used in their computations. The free stream Mach number was .08 and the Reynolds number based on flat plate length Re was $100.000/m$. The plate started at $x = .5$ and ended at $x = 3.2$ and was extended with a buffer region with slowly increased grid spacing to $x = 8.$ for the finite difference calculations and to $x = 5.$ for the finite volume calculations. The plate has 300 grid points in streamwise direction and the buffer region consisted of 36 points. The purpose of the buffer region was to damp out transients and thereby minimizing reflections. Accurate non-reflecting boundary conditions for the compressible Navier-Stokes equations are not yet available.

First a steady boundary layer solution was computed and the maximum pointwise value of the residual was less than 10^{-8}. The flow was then disturbed in a small region by periodic suction and blowing. The suction strip started at $x_1 = .908$ and ended at $x_2 = 1.13$. The amplitude is given by the relation:

$$f_v = A \sin(\tilde{x})(1 - \cos(\tilde{x})) \sin(\beta t)$$

with:

$$\tilde{x} = \frac{2\pi(x - x_1)}{x_2 - x_1}$$

The amplitude A for the computations is .0001. The parameter β is equal to 10, which results in a frequency parameter $F = 100$. Here the frequency parameter is defined as: $F = \beta \times 10^6/Re$.

The blowing and suction starts in the region were the boundary layer is linearly stable. This has as benefit that transients, which occur due to the suction and blowing, will damp out and a cleaner Tollmien-Schlichting wave is obtained. The time trace of all the flow variables along a line which corresponds to the position of maximum amplification was written to a file and Fourier analyzed. The Fourier analyzed signal was then used to compute the growth rate of the TS wave. Figure 3 shows the comparison of the growth rate $-\alpha_i$ of the streamwise disturbances with the results of Fasel et al.[5]. A negative value of the growth rate means that the disturbance is growing. The large initial disturbances are caused by the suction and blowing, but after $x = 1.4$ the result from the finite difference scheme compares well with that from Fasel et al.[5], which also agree with the theoretical non-parallel results of Gastner. The finite volume results are slightly less accurate than the finite difference results. This is partly due to the fact that the viscous contribution in the finite volume scheme is only second order accurate. The second simulation, a boundary layer at $M = 0.5$, which is at a considerably higher Reynolds number gives virtually identical results for both methods. The growth rates of the disturbances of the normal velocity component, Figure 4, also compare well with the results from Fasel et al.[5] , but the curves are shifted slightly upstream. This component becomes earlier unstable than in the simulation of Fasel et al.[5]. The growth rate of the normal velocity disturbances, however, strongly depends on the vertical position and further research is required to obtain more accurate results for this component. Contrary to the streamwise component there are no theoretical results for the growth rate of the normal velocity disturbances.

The same procedure as used for the $M = .08$ boundary layer was used for a simulation of a flat plate boundary layer at Mach number $M = .5$. The parameters were chosen equal to the calculations done by Bertolotti[2] using the linear Parabolic Stability Equations (PSE). This method takes the non-parallel effects of the boundary layer into account contrary to linear stability theory. The Reynolds number based on plate length was $500.000/m$. The simulations with the finite difference scheme were done on two grids. The coarse grid has 336×80 grid points and the plate started at $x = .5$ and ended at $x = 3.2$. Suction and blowing was started at $x = .725$ and ended at $x = .86$. The second grid con-

sisted of 436×80 points and the plate started at $x = .5$ and ended at $x = 2.3$. Suction and blowing started at $x = .5225$ and ended at $x = .6125$. The buffer region ends at $x = 8.$ for the coarse grid and at $x = 5.1$ for the fine grid. The first grid has about 10 grid points per TS wave and the fine grid has 20 point per wavelength. The frequency parameter F was equal to 20 and the free stream temperature $T_\infty = 206K$.

This case is more difficult than the incompressible simulation because of the higher Reynolds number and many more TS wave periods have to be covered. The initial amplitude of the disturbances A was .0001 and Figure 5 shows a contour plot of the pressure on the fine grid. The regular pattern of the TS waves is clearly visible. The initial amplitude is very small and decays, because the disturbance is in the stable part of the boundary layer. More downstream the disturbance grows very regularly, saturates and decays. The decay is partly physical and at the end of the plate further increased by the coarsening of the grid to minimize reflections from the outflow boundary.

Figures 6 and 7 show the spatial growth rates obtained with the finite difference and finite volumes scheme on the fine grid and compare them with the PSE results of Bertolotti[2]. They are virtually identical till the disturbances reach the buffer region, where the growth rate suddenly changes and the Tollmien-Schlichting wave rapidly decays. The CPU time used for both schemes was approximately equal for the implicit calculations, with the finite volume scheme 1.1 times more expensive than the finite difference scheme. The approximation of the flux integral in the finite volume method, equation (3.12), however, is crucial to minimize computing time for the finite volume scheme. These plots also show that the buffer region is quite effective in minimizing reflections from the outer wall. The simulation was continued in all cases till the leading wave front would have travelled at least twice the length of the domain. The sound waves, which travel faster, then would have a chance to reflect several times through the domain, with no apparent effect on the growth rates. The use of a buffer region is, however, not without pitfalls. One has to be very careful to create a smooth transition with the flow domain.

The accuracy of the simulation also depends on the time step and time integration scheme used. The time integration method is a second order 3 point implicit multi-step scheme. Four Newton iterations were used to improve time accuracy of the implicit scheme. The residue decreased two orders of magnitude during the Newton iterations and was approximately 5×10^{-7} at the end of the Newton iterations. Figures 8 and 9 show the growth rate of the normal and streamwise velocity component for simulations with different time steps using the finite volume scheme, but all on the 436×80 grid. The time step Δt is equivalent with a CFL number 80. As can be seen from these plots the accuracy is bounded by the time integration scheme and not by the spatial resolution. Significant improvement should be obtained by using a higher order accurate time integration method.

The results of computations with the finite difference scheme on the coarse and fine grid are presented in Figure 10. They show that the coarse grid simulation is underresolved, while the fine grid simulation compares well with the PSE results of Bertolotti[2]. It should be emphasized that it is very important to perform the computations on different grid levels to test accuracy, especially when there are no theoretical results available. The coarse grid results do show that the flow becomes unstable but the growth rate is not correct and can only be checked by increasing the resolution.

Finally, the effect of the location of suction and blowing was investigated. Figure 11. shows results of simulations with the finite difference scheme with suction and blowing applied directly after the inflow boundary or just before the region where the flow becomes unstable. It can be seen that the growth rates are not sensitive to the location of suction and blowing.

To summarize the results discussed in this section it can be stated that both the finite volume and finite difference schemes can be used for simulations of boundary layer instability. The results for the incompressible flow were slightly better for the finite difference scheme, but this can be attributed to the second order viscous contribution in the finite volume scheme. The biggest advantage of the finite difference scheme is that it is less sensitive to grid stretching, but this scheme is not easily extended to flows with sonic points, because it will loose accuracy at these points, which is not the case for the finite volume scheme. It was also found that using a higher order accurate time integration method will be more efficient and extreme care has to be taken to guarantee numerical accuracy, preferably by using grids with different resolution.

Acknowledgement

Part of this research was conducted during a stay at the Center for Turbulence Research, Stanford University. Sincere thanks are due to Professor J. Ferziger for helpful discussions and advice.

References

1. Abgrall, R. (1992), "On Essentially Non-Oscillatory

Schemes on Unstructured Meshes: Analysis and Implementation", ICASE Rep. 92-74.

2. Bertolotti, F. P., (1990), "Linear and Nonlinear Stability of Boundary Layers with Streamwise Varying Properties", Diss., Ohio State University, Columbus, Ohio.
3. Bestek, H., Thumm, A. and Fasel, H., (1992), "Direct Numerical Simulation of the Three-Dimensional Breakdown to Turbulence in Compressible Boundary Layers", Proc. 13th Inter. Conf. on Numer. Meth. in Fluid Dynamics", Rome.
4. Casper, J. and Atkins, H.L., (1993), "A Finite Volume High-Order ENO Scheme for Two-Dimensional Hyperbolic Systems", JCP, **106**, pp. 62-76.
5. Fasel, H. F., Rist, U. and Konzelmann, U., (1990), "Numerical Investigation of the Three-Dimensional Development in Boundary Layer Transition", AIAA J., **28**, pp. 29-37.
6. Godunov, S.K., (1959), "Difference Method of Numerical Computations of Discontinuous Solutions in Hydrodynamic Equations", Mat. Sbornik, **47**, pp. 271-306, Translated US Joint Publ. Res. Service, JPRS 7226, (1969).
7. Gottlieb, D. and Turkel, E., "Dissipative Two-Four Methods for Time Dependent Problems", Math. of Comp., **30**.
8. Harten, A. and Chakravarthy, S.R., (1991), "Multi-Dimensional ENO Schemes for General Geometries", ICASE Rep. 91-76.
9. Harten, A., Osher, S., Engquist, B. and Chakravarthy, S.R., (1987), "Uniformly High Order Accurate Essentially Non-Oscillatory Schemes III", JCP, **71**, pp. 231-303.
10. Herbert, Th., (1988), "Secondary Instability of Boundary Layers", Ann. Rev. Fluid Mech., **20**, pp. 487-526.
11. Laurien, E. and Kleiser, L., (1989), "Numerical Simulation of Boundary-Layer Transition and Transition Control", JFM, **199**, pp. 403-440.
12. Lax, P. and Wendroff, B., (1960), "Systems of Conservation Laws", Comm. on Pure and Appl. Math., **13**, pp. 217-237.
13. Lele, S. K., (1992), "Compact Finite Difference Schemes with Spectral-like Resolution", JCP, **103**, pp. 16-42.
14. Lee, S., Moin, P. and Lele, S. K., (1992), "Interaction of Isotropic Turbulence with a Shock Wave", Thesis, Stanford University, Rep. TF-52 Thermosciences Division, Dept. Mech. Eng.
15. Mack, L. M., (1984), "Boundary Layer Stability Theory", in "Special Course on Stability and Transition of Laminar Flow", AGARD Rep. 709.
16. Maestrello, L., Bayliss, A. and Krishnan, R., (1989), "Numerical Study of Three-Dimensional Spatial Instability of a Supersonic Flat Plate Boundary Layer", ICASE Rep. 89-74.
17. Osher, S. & Chakravarthy, S.R., (1983), "Upwind Schemes and Boundary Conditions with Applications to Euler Equations in General Geometries", JCP, **50**, pp. 447-481.
18. Osher, S. & Solomon, F., (1982), "Upwind Difference Schemes for Hyperbolic Systems of Conservation Laws", Math. of Comp., **38**, pp. 339-374.
19. Pulliam, T. H. and Chaussee, D. S., (1981), "A Diagonal Form of an Implicit Approximate Factorization Algorithm", JCP, **39**.
20. Rai, M. M., (1987), "Navier-Stokes Simulations of Blade-Vortex Interaction using High-Order Accurate Upwind Schemes", AIAA paper 87-0543.
21. Rai, M. M. and Moin, P., (1991), "Direct Numerical Simulation of Transition and Turbulence in a Spatially Evolving Boundary Layer", AIAA paper 91-1607-CP.
22. Roe, P. L., (1981), "Approximate Riemann Solvers, Parameter Vectors and Difference Schemes", JCP, **43**, pp. 357-372.
23. Shu, C.-W. & Osher, S., (1989), "Efficient Implementation of Essentially Non-Oscillatory Shock Capturing Schemes, II", JCP, **83**, pp. 32-78.
24. Steger, J.L. and Warming, R.F., (1981), "Flux Vector Splitting of the Inviscid Gasdynamic Equations with Application to Finite-Difference Methods", JCP, **40**, pp. 263-293.
25. Van Der Vegt, J.J.W., (1993), "ENO-Osher Schemes for Euler Equations", AIAA Paper 93-0335.
26. Van Der Vegt, J.J.W., (1991), "Assessment of Flux Vector Splitting for Viscous Compressible Flows", AIAA Paper 91-0243.
27. Van Leer, B., (1979), "Towards the Ultimate Conservative Difference Scheme V. A Second Order Sequel to Godunov's Method", JCP, **32**, pp. 101-136.
28. Van Leer, B, (1982), "Flux Vector Splitting for the Euler Equations", Proc. 8th Int. Conf. on Num. Meth. in Fluid Dyn., Berlin, Springer Verlag.
29. Vinokur, M., (1989), "An Analysis of Finite-Difference and Finite-Volume Formulations of Conservation Laws", JCP, **81**, pp. 1-52.

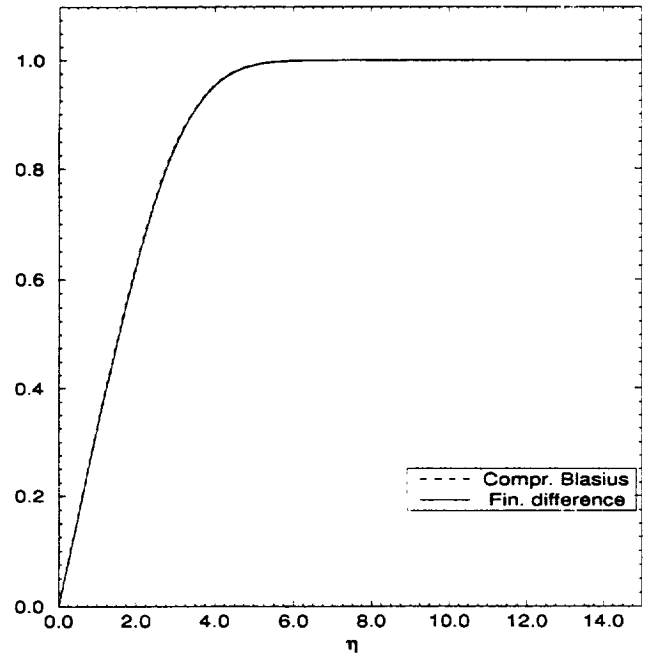

Figure 1. Streamwise velocity U at 10 equally spaced stations, $Re_x = 50.000 - 320.000$, $M_\infty = .08$, versus similarity parameter $\eta = \frac{y}{x}\sqrt{Re}$, compared with compressible Blasius solution (dashed line).

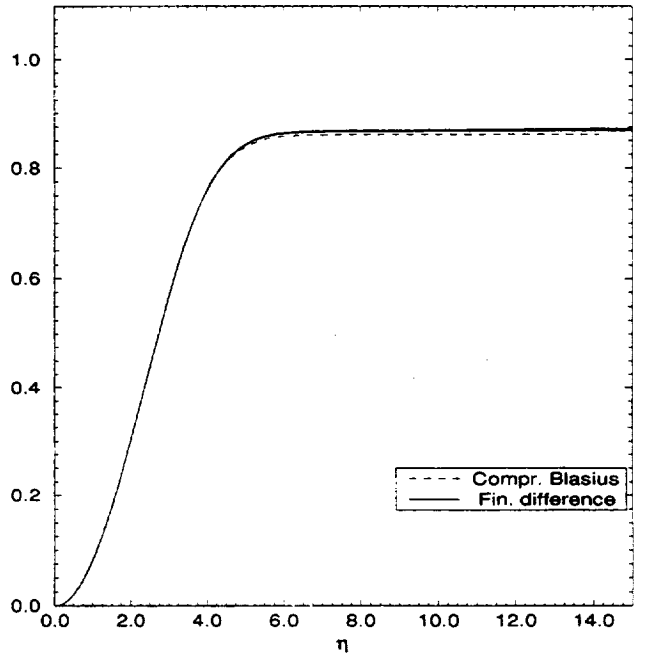

Figure 2. Normal velocity $V\sqrt{Re_x}$ at 10 equally spaced stations, $Re_x = 50.000 - 320.000$, $M_\infty = .08$, versus similarity parameter $\eta = \frac{y}{x}\sqrt{Re}$, compared with compressible Blasius solution (dashed line).

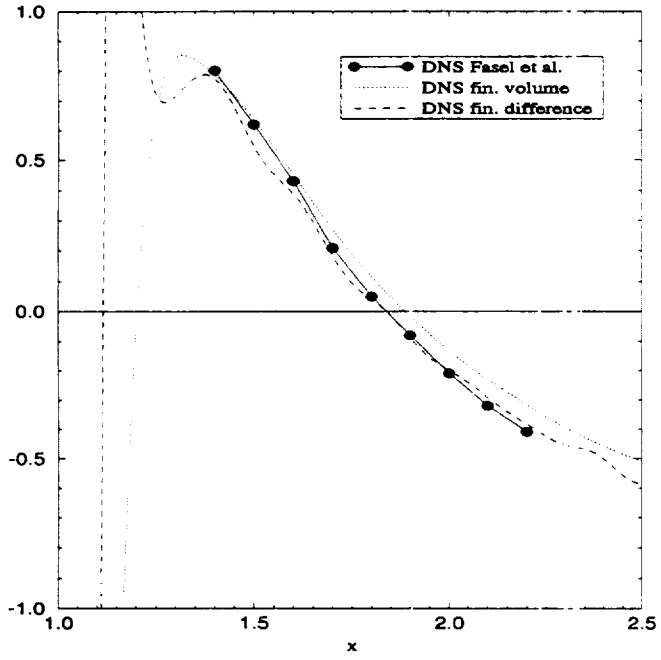

Figure 3. Spatial growth rate $-\alpha_i$ of streamwise velocity disturbances compared with results from Fasel et al.[5]. $M_\infty = .08$

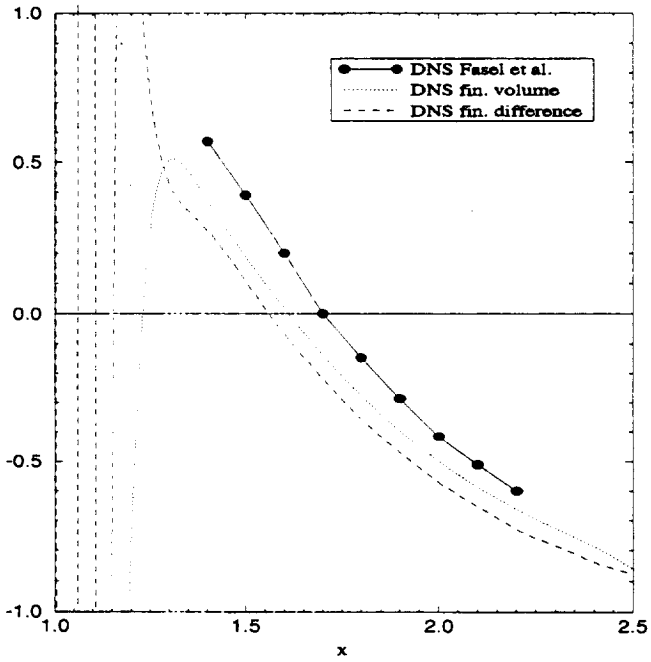

Figure 4. Spatial growth rate $-\alpha_i$ of normal velocity disturbances compared with results from Fasel et al.[5]. $M_\infty = .08$

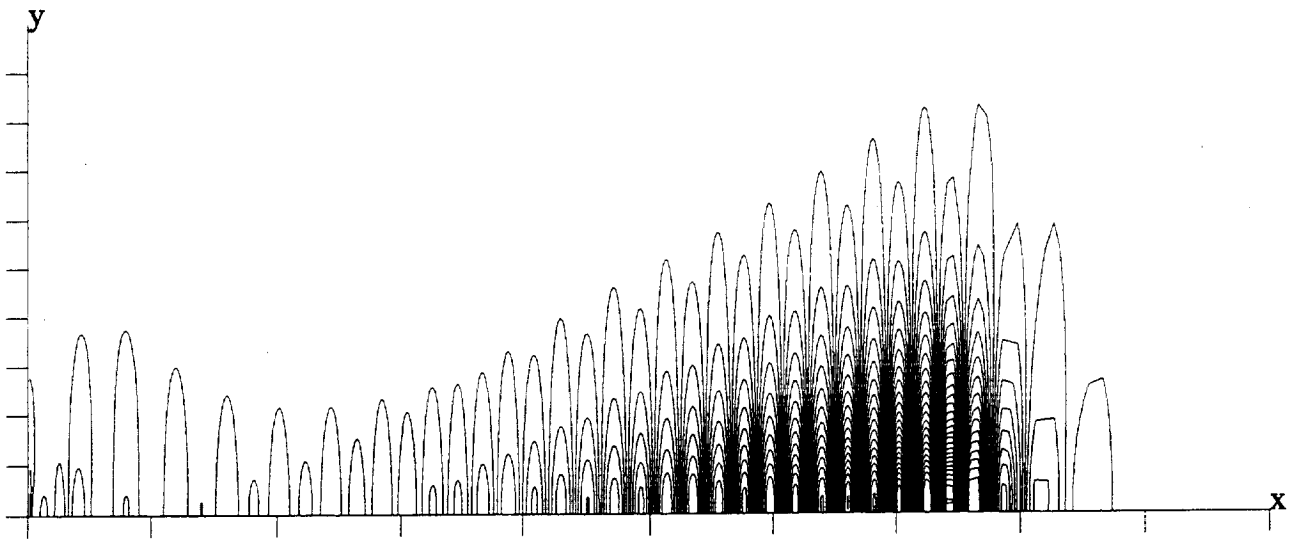

Figure 5. Pressure contours in flat plate boundary layer, $M_\infty = .5$, initial amplitude suction and blowing at wall .0001.

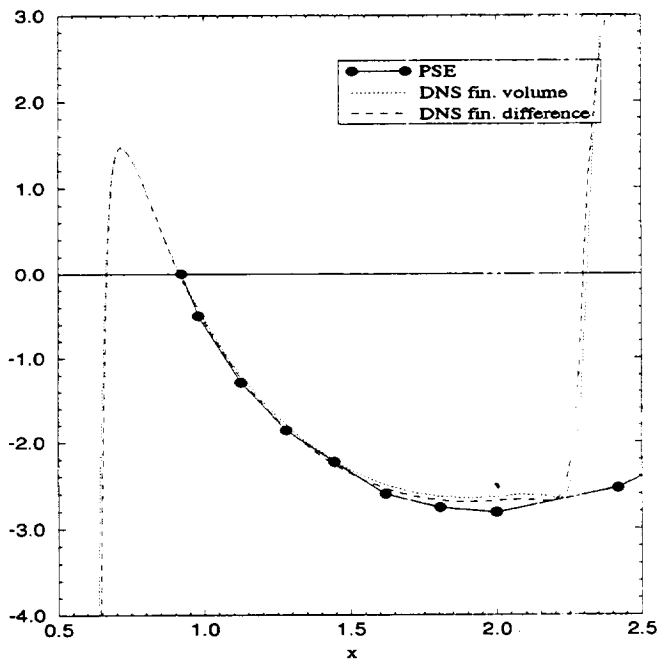

Figure 6. Spatial growth rate $-\alpha_i$ of streamwise velocity disturbances using finite volume and finite difference schemes compared with PSE results Bertolotti[2], $M_\infty = .5$

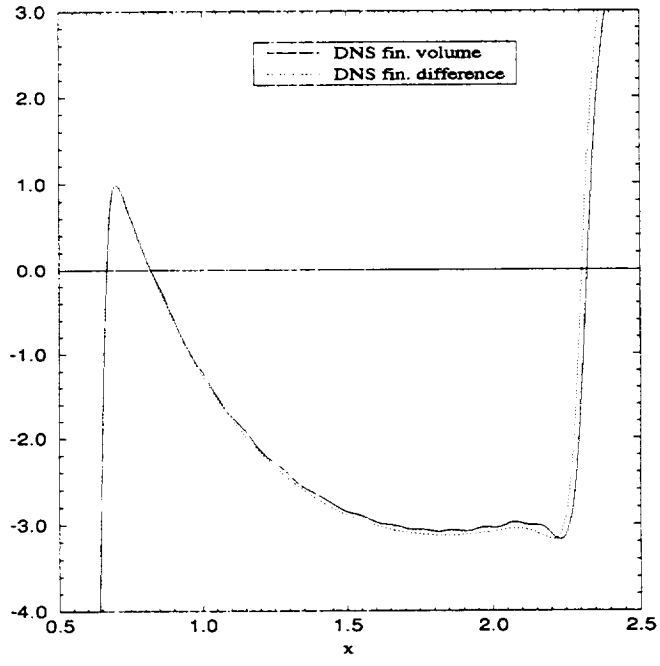

Figure 7. Spatial growth rate $-\alpha_i$ of normal velocity disturbances using finite volume and finite difference schemes compared with PSE results Bertolotti[2], $M_\infty = .5$

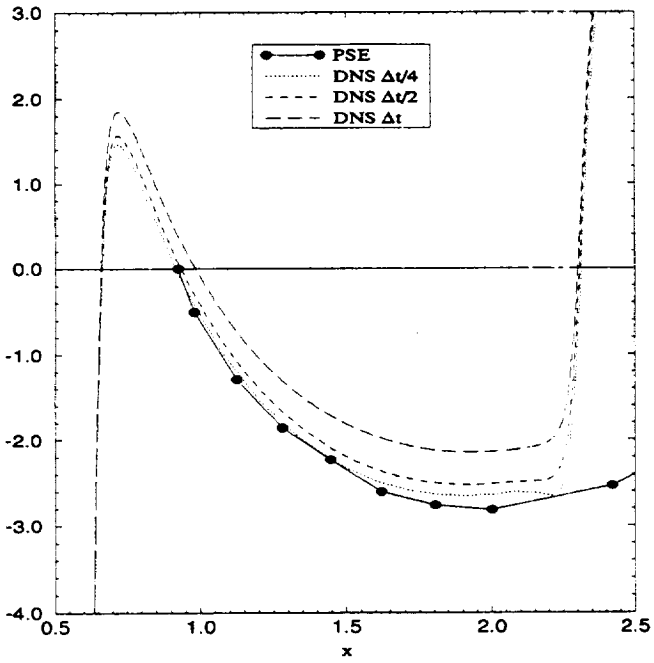

Figure 8. Spatial growth rate $-\alpha_i$ of streamwise velocity disturbances using finite volume scheme with different time steps, $M_\infty = .5$

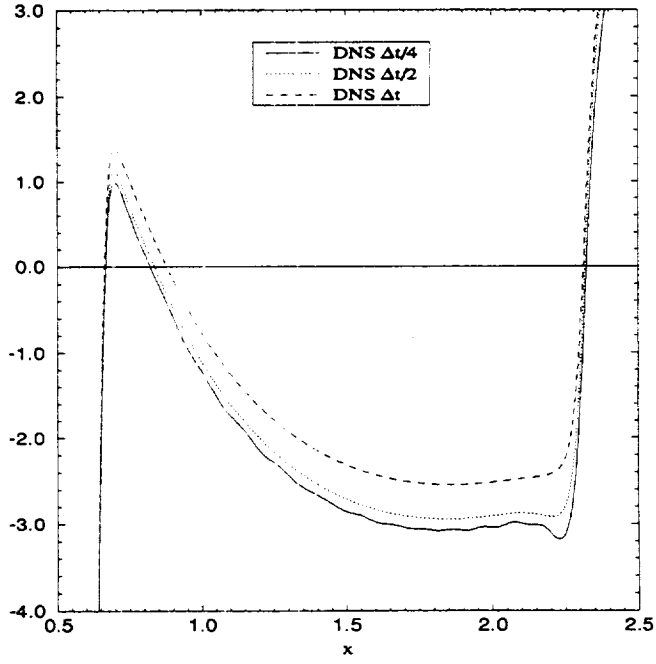

Figure 9. Spatial growth rate $-\alpha_i$ of normal velocity disturbances using finite volume scheme with different time steps, $M_\infty = .5$

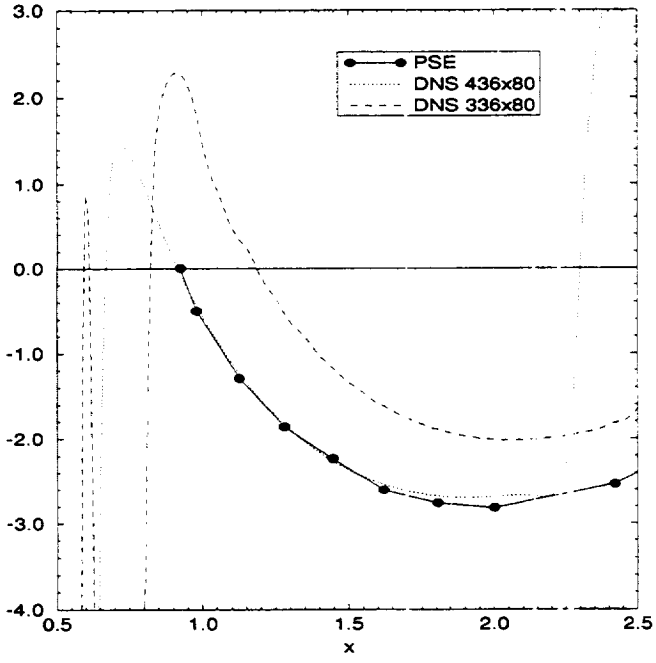

Figure 10. Spatial growth rate $-\alpha_i$ of streamwise velocity disturbances using finite difference scheme on coarse and fine grid, $M_\infty = .5$

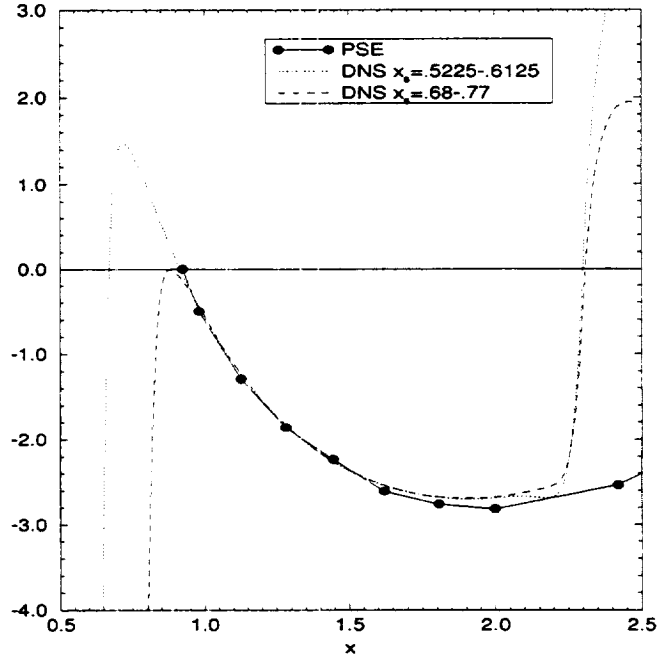

Figure 11. Spatial growth rate $-\alpha_i$ of streamwise velocity disturbances using finite difference scheme for different locations wall suction-blowing, $M_\infty = .5$

REPORT DOCUMENTATION PAGE

Form Approved
OMB No. 0704-0188

1. AGENCY USE ONLY (*Leave blank*)	2. REPORT DATE	3. REPORT TYPE AND DATES COVERED
	July 1993	Technical Memorandum

4. TITLE AND SUBTITLE

Higher-Order Accurate Osher Schemes With Application to Compressible Boundary Layer Stability

5. FUNDING NUMBERS

WU-505-90-5K

6. AUTHOR(S)

J.J.W. Van Der Vegt

7. PERFORMING ORGANIZATION NAME(S) AND ADDRESS(ES)

National Aeronautics and Space Administration
Lewis Research Center
Cleveland, Ohio 44135-3191

8. PERFORMING ORGANIZATION REPORT NUMBER

E-8139

9. SPONSORING/MONITORING AGENCY NAME(S) AND ADDRESS(ES)

National Aeronautics and Space Administration
Washington, D.C. 20546-0001

10. SPONSORING/MONITORING AGENCY REPORT NUMBER

NASA TM-106355
ICOMP-93-33; CMOTT-93-12
AIAA-93-3051

11. SUPPLEMENTARY NOTES

Prepared for the AIAA 24th Fluid Dynamics Conference sponsored by the American Institute of Aeronautics and Astronautics, Orlando, Florida, July 6-9, 1993. J.J.W. Van Der Vegt, Institute for Computational Mechanics in Propulsion and Center for Modeling of Turbulence and Transition (work funded under NASA Cooperative Agreement NCC3-233). ICOMP Program Director, Louis A. Povinelli, (216) 433-5818.

12a. DISTRIBUTION/AVAILABILITY STATEMENT

Unclassified - Unlimited
Subject Category 34

12b. DISTRIBUTION CODE

13. ABSTRACT (*Maximum 200 words*)

Two fourth order accurate Osher schemes are presented which maintain higher order accuracy on nonuniform grids. They use either a conservative finite difference or finite volume discretization. Both methods are successfully used for direct numerical simulations of flat plate boundary layer instability at different Mach numbers. Results of growth rates of Tollmien-Schlichting waves compare well with direct simulations of incompressible flow and for compressible flow with results obtained by solving the parabolic stability equations.

14. SUBJECT TERMS

Direct numerical simulation; ENO schemes; Boundary layer stability

15. NUMBER OF PAGES

16

16. PRICE CODE

A03

17. SECURITY CLASSIFICATION OF REPORT	18. SECURITY CLASSIFICATION OF THIS PAGE	19. SECURITY CLASSIFICATION OF ABSTRACT	20. LIMITATION OF ABSTRACT
Unclassified	Unclassified	Unclassified	